Modeling, design, and synthesis of gram-scale monodispersed silver nanoparticles using microwave-assisted polyol process for metamaterial applications

Z. Lalegani[1], S.A. Seyyed Ebrahimi[1*], B. Hamawandi[2], L. La Spada[3], M. S. Toprak[2*]

[1]Advanced Magnetic Materials Research Center, School of Metallurgy and Materials, College of Engineering, University of Tehran, Tehran, 11155 4563, Iran

[2]Department of Applied Physics, KTH Royal Institute of Technology, SE- 106 91 Stockholm, Sweden

[3]School of Engineering and the Built Environment, Edinburgh Napier University, Edinburgh, United Kingdom

[*]*Corresponding author e-mail: saseyyed@ut.ac.ir*

[*]*Corresponding author e-mail: toprak@kth.se*

Abstract

High-yield monodispersed silver (Ag) nanospheres were modeled, designed, and synthesized by microwave-assisted (MW-assisted) polyol method from $AgNO_3$, polyvinyl pyrrolidone (PVP), and ethylene glycol (EG), as precursors, at 145℃ within a short reaction time of 2 min, and the results were compared to those of conventional polyol method. Maintaining the PVP:$AgNO_3$ molar ratio, the effect of increasing the amounts of $AgNO_3$ and PVP at a constant amount of EG (40 mL) on the final product was evaluated. The synthesized nanoparticles (NPs) were characterized by SEM, UV-Vis spectroscopy, FTIR and DLS analysis. The results showed that with increasing the amount of $AgNO_3$ to 0.5 and 1 g, monodispersed Ag nanoparticles (Ag NPs) with particle sizes of 54 and 61 nm were formed, as per the plasmon absorption peaks at 436 and 442 nm, respectively. Moreover, using 40 mL of the EG solution, we could obtain a high yield of the NPs (~90%). The sub-gram yield was excellently high, offering great opportunities for commercializing the procedure. Also, the proposed study paves a new way for Ag NPs realization for different practical applications ranging from MW to optics.

Keyword: Microwave-assisted; High yield; Polyol; Silver NPs

1. Introduction

The development of plasmonic nanostructures have largely evolved the optics during the past couple of decades to the point where the design of optoelectronic sub-diffraction devices is now possible [1], opening new horizons for convenient manufacturing of metamaterials for various applications. The metamaterials are engineered composite materials that are made up of sub-wavelength particles called meta-atoms. Although such material could be used to adjust the electromagnetic response of a medium and hence gave birth to a complete new class of phenomena [2], their complicated architecture calls for complex nanofabrication methods including electron/ion beam lithography, which not only is costly and time-intensive but also suffers from fabrication limitations. The approach that has been recently investigated, both theoretically and experimentally, to overcome these limitations is the use of metallic NPs as meta atoms – the particles that exhibit plasmon resonance property and their size is small enough to act under a sub-wavelength regime [3]. Interaction of light with metallic NPs can lead to surprising effects that are significant in the context of technology. Excellent optical responsiveness of the metals roots in the forces generated as the incident light field reaches the almost free electrons of a metal and results in collective oscillation of electrons – photons. Strictly attached to the surface of the metallic NPs, these oscillations can induce sub-wavelength localization of the incident electromagnetic fields, which contributes to the formation of high-intensity regions around the plasmonic NPs and thus provides for conducting and controlling the light in the sub-diffraction range [4]. Localized surface plasmon (LSP) refers to the oscillation of free electrons within a metal particle, and the resonance frequency is the regulated plasma frequency by the particle size and shape. The LSPs can be found in engineered nanostructures and nanoparticle clusters and aggregates [5]. Technologically speaking, the plasmonic nanostructures (e.g. noble metal NPs) are very important for a range of applications including the photonics, optoelectronics, and biotechnology. Thanks to their size- and shape-dependent plasmonic properties, these nanostructures have been regarded by many researchers during the last decade. Noble metal-based plasmonic metamaterials (e.g. silver and gold NPs) exhibit extraordinary optical properties resulted from their localized surface plasmon resonance (LSPR) [6]. Designed logically, these structures offer excellent properties that cannot be found in naturally occurring materials. Here a coupling occurs between the photons and the conductive electrons of the metal, upon which the electrons go out of equilibrium state and the resultant tendency toward redistribution of the surface charge applies a restoring force onto the disordered electrons; the final result is an oscillation at a given frequency. When a dipole field is developed on the external surface of the NPs, another field is generated inside the particle. This significantly increases the adsorption and diffraction across the cross section, which is the main reason why the plasmonic NPs have been such largely regarded [1]. Among other metal NPs, the Ag nanostructures have been widely used in both technological and commercial research works. The Ag nanostructures constitute a primary metal element of metamaterials, and the low levels of loss associated with these structures have made them applied in high frequency metamaterials and a variety of applications including the near-field

optical probes, chemical and biological sensors, energy harvesting, SERS-based hyperbolic metamaterials for sensing (by which even singular molecules can be detected), imaging, and Raman scattering improvement for sensing applications [7-14]. Thanks to their wide spectrum of applications, these structures have been a major focus for the research works in the nanotechnology. These applications are highly dependent on the SPR, which is known to be controlled by the particle size and shape of the silver nanostructures [15]. Any tiny change in the synthesis condition can impose major impacts on the formation of NPs. Moreover, any alteration in the properties of the NPs can change the oscillation pattern of the free electrons and hence the resonance frequency. In this respect, a great deal of attention has been paid to various methods for synthesizing the AgNPs, leading to the emergence of numerous physical and chemical procedures for the synthesis of such NPs [7, 8, 16]. Among other methods, the most popular procedure for preparing the Ag NPs has been the chemical reduction of Ag ions by means of a reductive agent usually in presence of a stabilizer agent. As discussed in our previous work [17], the polyol process is one of the best and most convenient methods for reducing the Ag ions. However, since the electronic and optical characteristics and, especially, the LSPR of the Ag NPs is highly dependent on the particle size and shape, the need for stabilization and size distribution/dispersion of the NPs in the host matrix has given rise to a number of novel synthesis strategies that affect the dispersity of the NPs [18, 19]. Therefore, the necessity of modifying the polyol method to achieve uniformly distributed monodispersed particles is pretty obvious. Form another point of view, the development of the NPs from the laboratory to the market is progressing at a low pace. This requires that the method for producing the NPs be well scalable and repeatable [20]. The conventional heating method adopted in many synthesis procedures results in a nonuniform out-of-control nucleation stage that ends up with a relatively wide range of particle sizes and morphologies, i.e. nonuniform growth of the NPs [21].

The microwave (MW) technology has been rapidly developed during the past years [22]. It has been because of the unique effects of the MW that could trigger interactions in chemical media to achieve a wide range of results [23]. Compared to conventional heating methods, the MW-assisted heating provides for a higher reaction rate, significantly shortens the crystallization time, and contributes to homogeneous nucleation, higher yields, and economic efficiency [24, 25]. As of present, many synthesis methods, including the green synthesis method, have utilized the power of MW for synthesizing Ag NPs. The use of MW energy in the polyol synthesis method has made it possible to obtain Ag NPs of various shapes, including nanowires, nanoplates, and nanoprisms [26-29]. In all of such research works, the researchers were seeking to achieve uniform Ag NPs at the highest possible yield [30-32]. The MW-assisted synthesis can be scaled up to accelerate the commercialization of the NPs. Using the MW-assisted polyol method, Torras and Roig [20] could improve the yield of NP production to 61%, obtaining 1 mg of silver per batch. Following a similar approach, Helmlinger et al. [31] obtained 20 mg of Ag per batch, corresponding to a yield beyond 98%. Kumar et al. [33] presented a MW-assisted synthesis route for Ag NPs, < 10 nm, using starch and sugar as capping and reducing agents. They used a reaction time of 4.5 min and reported almost complete conversion.

In the present work, a new circuit modeling approach for NPs had been proposed, and the MW-assisted polyol method was used to obtain Ag NPs at a significantly higher yield than previous works. Moreover, with increasing the amount of the silver precursor to 1 g, we extracted some 0.6 g of silver per a 40mL batch of EG, corresponding to a yield of about 90%. The obtained yield corresponded to a significant fraction of a gram, which was very large compared to similar works and definitely unprecedented. Moreover, compared to other research works, the obtained NPs enjoyed higher degrees of monodispersity and more uniform particle size distribution.

2. Modeling and design of AgNPs

An incident electromagnetic/thermal wave can impinge on a nanosphere with radius $\boldsymbol{r}$, electric permittivity $\boldsymbol{\varepsilon}$, and thermal conductivity $\boldsymbol{k}$, that immersed in a homogeneous medium ($\boldsymbol{\varepsilon_r}, \boldsymbol{k_r}$). A schematic is shown in figure S1. The electromagnetic/ thermal fields inside and outside the nanosphere can affect on the nanosphere polarizability [34]. In this work, we consider single particles, and electric/thermal polarizability is expressed as follow:

$$\alpha = \frac{V\delta_0(\delta_1 - \delta_0)}{\delta_0 + L(\delta_1 - \delta_0)} \quad (1)$$

Where $\boldsymbol{\alpha}$ is polarizability, $\boldsymbol{V}$ is the particle volume, $\boldsymbol{L}$ is the particle depolarization factor ($L = \frac{1}{3}$ for sphere), $\boldsymbol{\delta_i}$is the thermal conductivity (or the electric permittivity $\boldsymbol{\varepsilon_i}$); $\boldsymbol{i}$=0, 1 for environment and NP, respectively.

If there is more than one NPs, with radii $\boldsymbol{r_1}$and $\boldsymbol{r_2}$, electric permittivity $\boldsymbol{\varepsilon_1}$and $\boldsymbol{\varepsilon_2}$, thermal conductivity $\boldsymbol{k_1}$ and $\boldsymbol{k_2}$, and with a certain distance $\boldsymbol{d}$, one can consider a coupled-circuits, each depicting one of the NPs. Each circuit include a dependent voltage indicating the influence of the electric/thermal field of the other particle(s); and hence, the interaction among the particles can be modeled, as shown in figure S1.

We evaluated the electromagnetic wave components starting from the Ag NP polarizability expressions inside and outside the structure according to the sphere geometry. Figure 1 shows the electric and thermal field distribution for the single sphere and across the spheres. More information about the design and modeling is available in the supplementary file.

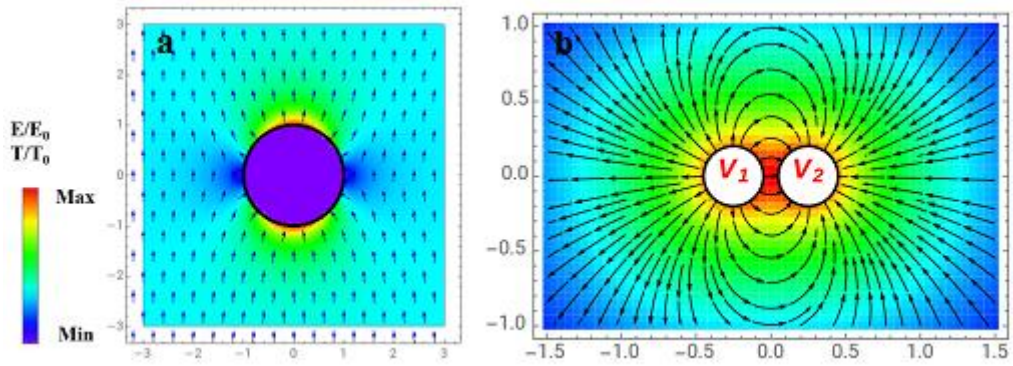

Figure 1. a) Electric and thermal field distribution for the single sphere: field arrows (analytical results) and colors (full-wave simulations) represent the fringe dipolar electric/thermal field, b) electric and thermal field distribution across the spheres: field arrows (analytical results) and colors (full-wave simulations) represent the dipolar electric/thermal coupling field.

The new circuit modeling approach had been proposed in this study, permits to have full control of the electromagnetic and thermal properties of AgNPs for required applications. We will use our modeling coupling effect across Ag NPs at different distances for a fixed Ag NP and will use these properties to compare with experimental results that will be presented in our future work. In the following, we have tried to synthesize uniform and monodisperse AgNPs with size under 100 nm by a MW-assisted polyol process.

3. Experimental

3.1. Materials and instrumentation

Silver nitrate ($AgNO_3$, crystal extra pure, Merck, Sweden), polyvinyl pyrrolidone -PVP (K30, PanReacAppliChem), and ethylene glycol-EG ($C_2H_6O_2$, Sigma Aldrich, Sweden) were used as Ag precursor, capping agent, and reducing solvent, respectively.

The synthesis of AgNPs was performed via MW-assisted heating process (flexiWAVE-Milestone, 1800 Watt; equipped with multivessel high pressure rotor). Morphology of AgNPs was characterized using scanning electron microscopy (SEM- FEI Nova200, Hillsboro, OR, USA). Average size of AgNPs was determined using ImageJ software, based on the calculated area of minimum 100 particles per sample. Particle size distribution was calculated by fitting a Gaussian function to the data in Origin software (version 8.6.0.70). Also, the hydrodynamic size of AgNPs were measured by dynamic light scattering (DLS-MalvernZetasizer Nano ZS90). UV-Vis spectrophotometry (ImplenNanoPhotometer, NP80) was performed to obtain SPR spectra of colloidal AgNPs. Fourier-transform infrared spectroscopy (FT-IR, Thermo Scientific Nicolet iS20) was used to obtain FT-IR spectra in transmission mode on KBr pellets, by drying a drop of Ag NP colloid in ethanol on the pellet, in the spectral range of 4000 - 400 cm^{-1}.

3.2. Synthesis of Ag NPs

Inspired by our previous work on the synthesis of Ag NPs through the conventional polyol method [17], a novel MW-assisted polyol method is herein proposed for synthesizing Ag NPs. Table 1 lists the concentrations of the precursors in the synthesized samples. For the sample N1, firstly, PVP was added to 40 mL EG at 70℃ under stirring to obtain a clear solution, which was left at room temperature for cooling. Next, $AgNO_3$ was added to the solution under stirring to have it well dissolved in the solution. When it came to the samples N2 and N3, a different dissolution method was used for dissolving the PVP and $AgNO_3$ in the EG due to the high concentrations of the precursors, as the precursors could not be dissolved under normal stirring at 70℃. For the two latter samples, appropriate amounts of PVP and $AgNO_3$ (Table 1) were simultaneously added to 40 mL of EG and then completely dissolved using an ultrasound probe in a couple of minutes.

The prepared solutions were transferred to the vial of the MW apparatus. The program for MW-assisted heating under stirring was as follows. The solution was subjected to MW-assisted heating to achieve 145℃ in 1 min. Then, the temperature was held for 2 min before the solution was cooled down to the room temperature. The obtained solution was then centrifuged at 12000 rpm for 30 min. The obtained NPs were three-times washed with ethanol and then precipitated by centrifuging at 12000 rpm for 10 min. They were then dispersed in ethanol for subsequent characterization.

Table 1. Precursors concentrations used for the synthesis of various AgNP samples.

Sample	$AgNO_3$ (g)	PVP (g)	EG (mL)	PVP/$AgNO_3$ (mole ratio)
N1	0.1	0.4	40	6
N2	0.5	2	40	6
N3	1	4	40	6

4. Results and discussion

4.1. MW-assisted synthesis and comparison with conventional polyol process

In our previous work, we designed a synthesis method by means of conventional polyol method using the RSM-BBD to achieve spherical AgNPs of desired particle size [17]. Using the formulated design, the optimal ranges of the parameters affecting the final product were also determined. Results of the design methodology, some of which are demonstrated in Figure 2 and which were thoroughly interpreted in the previous work [17], showed that the PVP surfactant concentration affects the size and shape of the Ag NPs significantly.

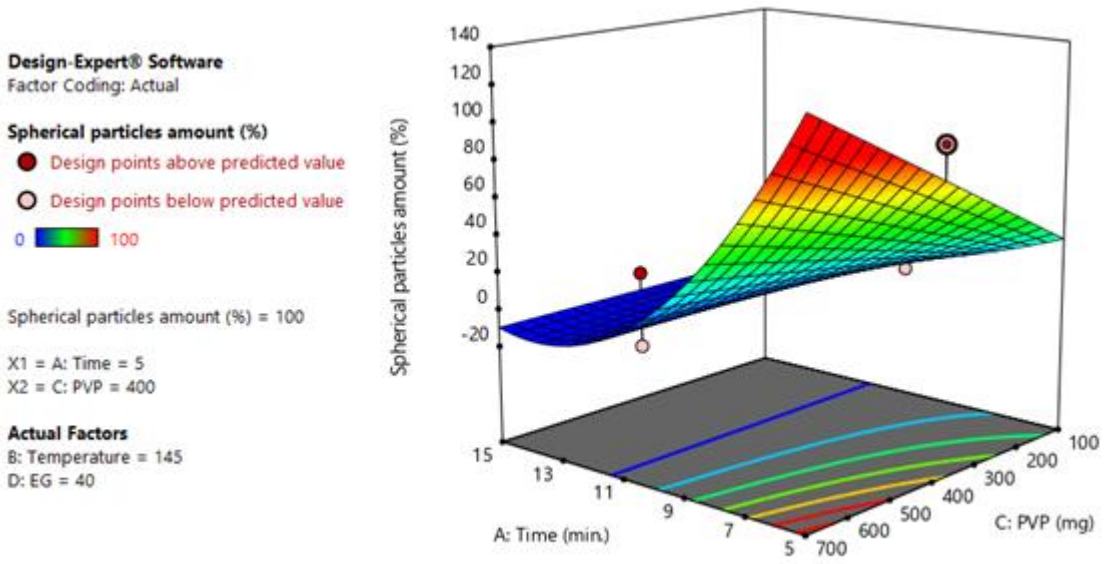

Figure 2. 3D plot of combined effect of PVP concentration and reaction time on the percent of spherical AgNPs at temperature of 145℃ and 40mL EG using conventional polyol synthesis route.

Despite the good results in terms of the control over the size and shape of the Ag NPs using the conventional polyol method, the methodology suffered from major drawbacks including low yield and agglomeration of NPs mainly due to the heating method adopted for warming up the reaction mixture. In order to address this problem, we modified the heating technique for the polyol method to MW-assisted heating (MW-assisted polyol method). Accordingly, for comparison purposes, from our previous work the S19 sample (5min/145℃/0.4g PVP/0.1g $AgNO_3$/40mL EG) [17] was selected for the synthesis of NPs through the MW-assisted polyol method. Therefore, a solution composed of 0.1g of $AgNO_3$, 0.4g of PVP, and 40 mL of EG was selected for heating at 145℃, just like the S19 sample, with the only difference being the MW-assisted heating time that was herein set to 2 min. Figure 3 shows the heating profiles of various solutions during the course of the synthesis of Ag NPs via the MW-assisted and conventional polyol methods.

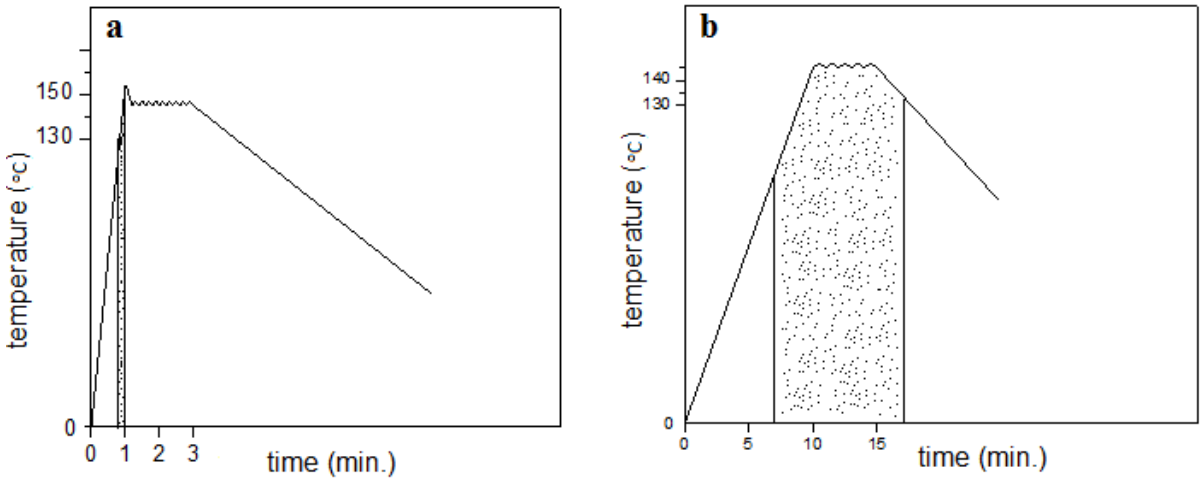

Figure 3. The schematic of heating profile of solutions during the synthesis of AgNPs by polyol method using a) MW heating, and b) conventional heating (hot plate). Dotted regions are likely representative of nucleation and growth process.

According to figure 3, the solution temperature reached 145℃ within 1 min of the MW irradiation, while the conventional method required about 10 min to raise the solution temperature to the desired point. This is because the heat was initially transferred to the walls of the reaction plate rather than the core of the solution in the conventional heating. This was while the MW-assisted heating tended to directly heat those precursors of the reaction mix that were susceptible to MW polarization. This direct heating method boosted the kinetics of the reaction and increased the sample temperature at a much faster pace than the conventional method. Therefore, a major advantage of the MW-assisted method was its ability to increase the heating rate of the reaction mixture significantly. Depending on the types of reactor and the precursor molecules, the heating rate could be as high as 30℃/s thanks to high energy absorption by the reaction mixture as the MW could penetrate into the volume of the solution and generate heat by means of direct interactions with the matter [35-37]. In the course of these interactions, the heat production occurred inside the material by means of the MW-developed electromagnetic fields at atomic level. As the material was hit by the MW, its rotational modes were excited and energy absorption occurred via the resonance phenomenon. Moreover, knowing that the rotational – vibrational excitations are principally specific to chemical reactions, the MW played an important role in the chemical reaction [38-40]. The ability of the reaction mixture to effectively absorb the MW energy determines the behavior of MW-assisted chemical reactions. This energy absorption is a result of the interaction between the electrical component of the MW and the charged dipoles or particles in the solution, largely depending on the choice of solvent for the reaction [36, 41]. The response of the solvent to oscillating MW fields are described by the dielectric constant, ε*, as follows:

$$\varepsilon^* = \varepsilon' - j\varepsilon'' \qquad (2)$$

Where ε' is the polarizability and $\varepsilon''$is a measure of the material's ability to dispose, absorb, and convert the MW energy into the heat. These are basic parameters for expressing the dielectric heating, and their ratio is called the loss factor,$tan\delta = \frac{\varepsilon''}{\varepsilon'}$ an important metric for comparing the efficiency of different materials for converting the MW energy into heat. Accordingly, higher values of $tan\delta$indicate larger capacity of the solvent for absorbing the MW energy. In this respect, a solvent with a $tan\delta > 0.5$ provides a good MW absorber [41]. Before the solvent molecules can convert the MW energy into the heat, the molecules must not only align with the oscillating electromagnetic field, but also rapidly recover their irregular state before a new field is applied. The molecular friction occurred under such circumstances represents a principle step along the path to generate heat. Called relaxation (τ), this capability determines the loss factor ($tan\delta$) [42, 43]. In the MW-assisted chemistry, the best solvents are bipolar molecule-bearing liquids. Thanks to their high viscosity, the alcohols containing OH groups attached to carbon backbones can form hydrogen bonds, contributing to the generation of group moments and long relaxations (τ). The high value of $tan\delta$ for these solvents is very significant [36, 43, 44]. With a $tan\delta$ beyond 1 (i.e., 1.35) at 2.5 GHz, ethylene glycol (EG) is an excellent reducing solvent for the synthesis of metal NPs through the MW-assisted polyol route.Results of previous studies have shown that dielectric loss of EG is maximal in the frequency range of 1.28 – 4 GHz. Sengwa et al. [45] investigated the effect of chain length of ethylene glycols on their dielectric properties at different temperatures from 25℃ to 55℃. They measured the dielectric loss ε'' of EG using a vector network analyser and they plotted the values of ε'' versus frequency. Their experiments results show a maximum of ε'' at the frequencies of 1.64 GHz, 2 GHz, 3 GHz, and 4 GHz at temperatures of 25℃, 35℃, 45℃, and 55℃, respectively. Also, Undre et al. [46] measured the dielectric properties of EG at 20℃. We can see the dielectric loss peak for EG in the frequency range from approximately 1.2 to 2 GHz.

The behavior of the EG under MW irradiation depends on not only the dipole moments, but also short-range interactions such as intermolecular hydrogen bonding, also known as Kirkwood factor ($\boldsymbol{g}$). When a group of molecules tend to get aligned with parallel dipole moments, the value of $\boldsymbol{g}$ will exceed 1. That is, the molecules have their freedom reduced for re-orientation and the value of τ increases [41, 45], which means that the solvent performs better. For EG at 25℃, the values of $\boldsymbol{g}$ and $\boldsymbol{\tau}$ are 2.37 and 92.4 ps (i.e., within the allowed range for effective coupling at MW frequency; 51.5 – 800 ps), respectively [43, 47]. These findings show that EG is an excellent solvent for dielectric heating. Decomposition of silver nitrate and reduction of Ag^+ occur under MW irradiation in EG. Accordingly, upon dehydration of EG, through which it converts to its acetaldehyde form, the Ag^+ ions are altered to atomic Ag, and the primary product of the oxidation of EG via the following reaction is the diacetyl [48, 49]:

$$AgNO_{3(s)} \rightarrow Ag^+ + NO_3^-$$

$$HO - (CH_2)_2 - OH \rightarrow CH_3CHO + H_2O$$

$$Ag^{+} + 2CH_3CHO \rightarrow CH_3 - \underset{\underset{O}{\|}}{C} - \underset{\underset{O}{\|}}{C} - CH_3 + H_2 + Ag$$

These reactions occur because of the increased temperature of EG upon the MW irradiation. The MW irradiation possesses energy levels in the range of 1 J/mol, which is inadequate for breaking chemical bonds (e.g., hydrogen bonds require 4 – 42 kJ/mol of energy to break apart). Therefore, the MW energy is nonionizing, meaning that it can act at molecular level only rather than changing the material structure [50, 51]. According to the methodology proposed by Kumar et al. [33], the energy applied to the solution in the present work was calculated as 54 kJ considering the MW power (here 1800 W), number of reaction vessels, volume of reaction mix per vessel. This was while the free energy of activation of the dipole relaxation process with EG was as low as about 16 kJ/mol. The torques experienced by the dipoles at the MW-range frequencies make them physically spin and continuously change as a result of the resultant thermal agitation, so that they can respond to a reverse field for up to 10^6 times per second. The loss tangent of this organic solvent, which exhibits a relaxation time beyond the 65 ps at a frequency of 2.45 GHz, increases with temperature [43,45], so that the solvent can convert greater than expected amounts of the MW energy into heat energy, and the molecules do not turn randomly oriented immediately upon turning the field off. This can be a reason to the increase in temperature from 145℃ to 155℃ in figure 3a. Fast spinning of a molecule can increase the inductive energy transfer to adjacent molecules, resembling some impact into the adjacent molecules. Therefore, according to the Arrhenius equation for a rate constant *k*:

$$k = A\, exp\left(-\frac{\Delta G'}{RT}\right) \qquad (3)$$

It is believed that the electrical field component of the MW irradiation can increase the rate of contact between the reaction molecules (*A*) [36]. Thus, the activity of a chemical reaction under a given thermal condition can go beyond the expectation. For the EG, in addition to the dipole spinning mechanism, the ionic conductivity can also serve as an interaction process that contributes to the MW-assisted heating process. The ionic conductivity is known to increase with temperature, making the temperature an important parameter determining the relative contribution of this mechanism. At 25℃, the relaxation time of the ionic conductivity of the EG (τ_σ) was about 1.99 μs [47, 50], while the corresponding relaxation time to the dipoles was 92.4 ps. Therefore, in the beginning of the reaction, the spinning of the dipoles was the dominant driver of the heating process. Moreover, knowing that the temperature reached 145℃ during the tests, which was not enough to activate the reductive function of EG, then it can be stipulated that the dominant mechanism of heating the solution was the dipole spinning. In this respect, the heating process was uniform and beyond the conventional heating method, as demonstrated in figure 3, leading to rapid decomposition of the $AgNO_3$ molecules and formation of a high monomeric super saturation for triggering the homogeneous nucleation of Ag NPs; this is the most important effect of the MW-assisted heating for the synthesis of Ag NPs. The MW irradiation tends to heat the reaction solution homogeneously, which results in uniform nucleation followed by a rapid crystal growth. The

performance of the EG as a reducing agent is maximized at temperatures near its boiling point (> 170℃), leaving it reportedly ineffective for reducing the Ag^+ ion at lower temperatures, even in the range of 100℃ [52].

According to our experiments, no Ag NP was observed at temperatures below 130℃; this made us consider 130℃ as the starting temperature for nucleation process (Figure 3). Due to reasons mentioned earlier, most frequently, the active sites for reducing the Ag^+ through MW irradiation are activated at the same time; this makes the reduction process well controllable and contributes to the formation of Ag nuclei at high density. Based on figure 3a, the temperature raised from 130℃ to 145℃ in less than a minute, in which temperature region many nucleation sites were developed simultaneously followed by fast-pace growth of the Ag NPs. This is while the nucleation process through the conventional synthesis method (Figure 3b) takes a couple of minutes to reach a temperature of 145℃ as the heating is done at a limited thermal gradient; moreover, in the conventional approach, the solution in contact with the vessel wall is heated sooner than the solution in the middle of the vessel. This nonuniform heating profile then leads to continuous and nonuniform nucleation of the Ag NPs in the solution. The fact that the reaction vessel wall is usually ended up silver coated when the conventional synthesis method is applied confirms the non-uniform nature of the nucleation process. In a research on the effect of the MW irradiation on the nucleation and crystal growth, Jhung et al. [35] proved that the effect of the MW energy is more emphasized on the nucleation stage rather than the crystal growth. Indeed, simultaneous activation of the nucleation sites contributes to the uniform occurrence of the nucleation in less than a second, while the conventional synthesis method leads to a situation where nucleation process continues as long as the EG temperature is appropriate for the chemical activity. According to figure 3b, such condition may continue to hold even during the cooling stage of the solution, eventually leading to nonuniform distribution of Ag NPs. Figure 4 shows the SEM micrographs of the synthesized Ag NPs through both MW-assisted and conventional methods.

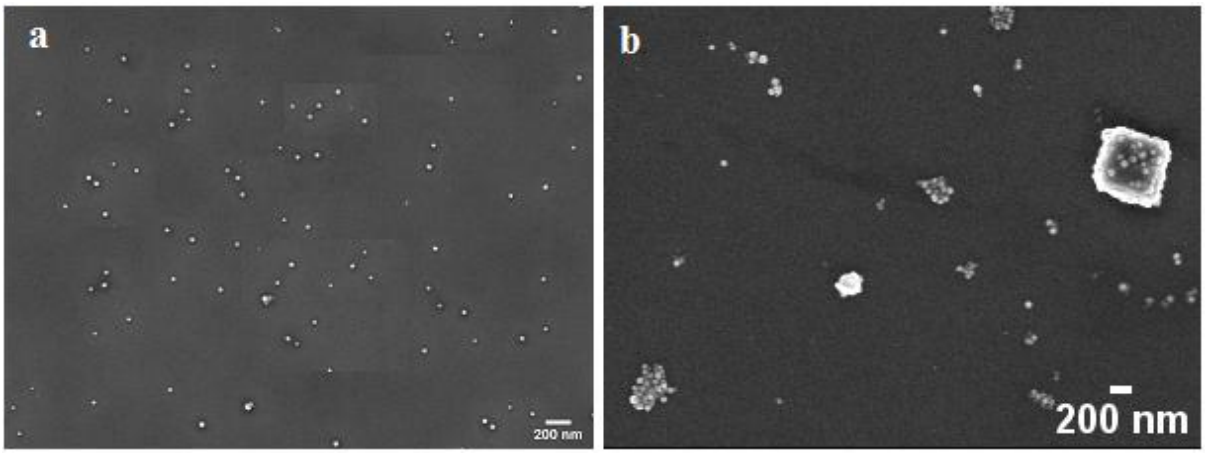

Figure 4. SEM micrographs of AgNPs synthesized by a) MW-assisted polyol process (under conditions 2min/145℃/0.4g PVP/0.1g $AgNO_3$/40mL EG), and b) conventional polyol process (under conditions 5min/145℃/0.4g PVP/0.1g $AgNO_3$/40mL EG).

As observed in figure 4a, with the MW-assisted synthesis method, the Ag NPs were near spherical in shape and well dispersed through the solution with a uniform distribution. The conventional synthesis method (Figure 4b) led to a mass of agglomerated NPs as a result of the nonuniform nucleation of Ag NPs in EG, with the quantity of synthesized NPs being generally very small. Moreover, the fact that the amorphous regions were far from the crystal nuclei, and the number of nuclei was generally low, led to agglomeration of the NPs and the massive growth of them. The conventional synthesis method led to Ag NPs with a primary particle size of about 50 nm, while some giant particles in the order of 500 nm were observed that is ascribed to significant particle growth. In the MW-assisted technique NP size was about 30 nm Ag NPs. In addition, given that the synthesis process time is very short with the MW-assisted technique, it seemed that no significant change was occurred into the NP size and shape throughout the whole process, with the only changes being the significantly higher yield and monodispersity of the particles, as was confirmed by comparing the UV-Vis spectra of the colloids made via both methods (Figure 5). Indeed, the symmetric and narrow spectrum observed for the Ag NPs synthesized via the MW-assisted method indicated the uniform nucleation and growth of the Ag NPs and their uniform particle size distribution. The symmetric peak observed at 422 nm highlighted the presence of uniform Ag NPs with an average particle size of 30 nm. This was while the conventional synthesis method led to two peaks at 442 nm and 694 nm (see supplementary Material figure S3), indicating the larger size and extensive agglomeration, or large Ag nanocrystals.

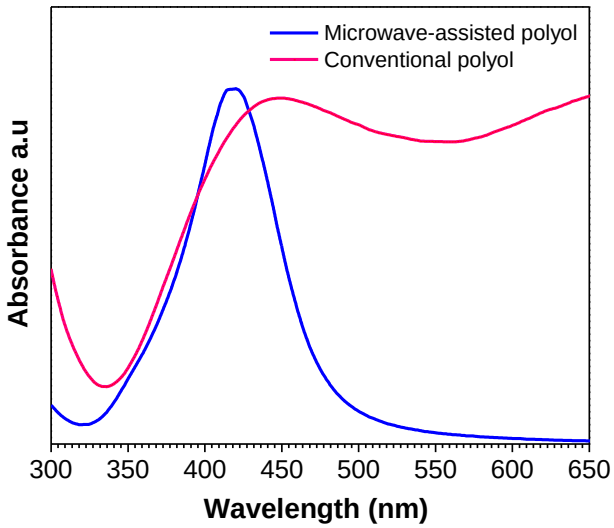

Figure 5. UV-Vis spectra of AgNPs synthesized by MW-assisted and conventional polyol processes (The max intensity is normalized to make the comparison easier).

4.2. Scaling up the amount of Ag NPs with MW-assisted synthesis method

Considering the previous section and taking the conventional reactions as a baseline, the reaction engineering and technical parameters are seen to play a greater role in the MW-assisted reactions [51], providing for scale-up of the process to achieve larger amounts of the products. For this purpose, a conventional reaction was repeated under MW irradiation under a known set of conditions, and acknowledging the acceptable results in terms of shorter reaction time and higher yield and quality of the synthesized NPs, it was decided to increase the amount of the precursor without changing the amount of solvent. According to Table 1, preserving the PVP/$AgNO_3$ molar ratio, the amount of $AgNO_3$ was increased to 5 and 10 times as large as the original amount (0.5 and 1 g, respectively). Solving such large amounts of the nitrate and PVP in the EG was found to be impractical using the conventional hot-plate method and only became possible when an ultrasonic nozzle was utilized. Upon dissolving the precursors, a large amount of Ag NPs was produced within only 2 min. Figure 6 shows the SEM micrographs of the synthesized Ag NPs and their particle size distributions for the synthesized samples. The yield of the MW-assisted synthesis reaction was calculated as 90% for Ag NPs studied herein. This means obtaining 0.3g and 0.6g AgNPs per 40 mL of solution with different concentration of $AgNO_3$, while Kumar et al. [33] reported a yield of > 99, synthesizing about 0.026g of AgNPs per 20 mL batch. The typical batch in our process yields about 20 times higher quantity of Ag NPs. This combined with the rather short reaction time shows the promise of our approach in terms of energy efficiency.

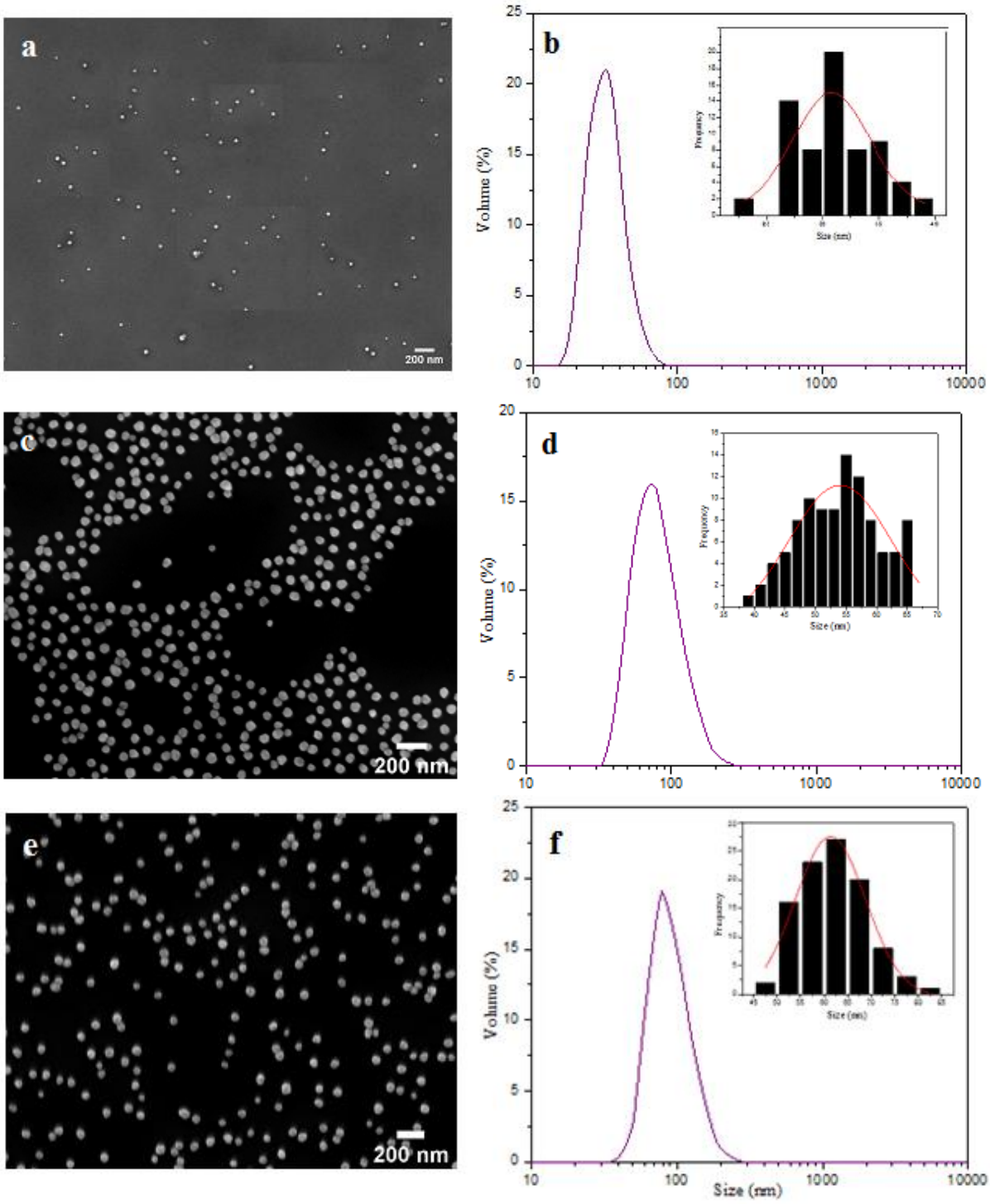

Figure 6. a) SEM micrograph, and b) particle size distribution by DLS and ImageJ (inset) of AgNPs for sample N1; c) SEM micrograph, and d) particle size distribution by DLS and ImageJ (inset) of AgNPs for sample N2; e) SEM micrograph, and f) particle size distribution by DLS and ImageJ (inset) of AgNPs for sample N3. For sample designations see table 1.

The SEM micrographs evidently show the large population of the synthesized NPs, their uniform particle size distribution, and mono dispersity across the solution, confirming the

accelerated nucleation and crystal growth under the effect of MW irradiation. Physical properties of the synthesized NPs are listed in table 2.

Table 2. Physical properties of synthesized AgNPs including the position of the surface plasmon resonance (SPR) peak, average NP size estimated from SEM, UV-Vis and DLS techniques, along with the polydispersity index (PDI) for DLS measurements.

Sample	SPR peak [nm]	SEM, ImageJ		Size (UV-Vis) [53] [nm]	DLS	
		Size [nm]	PD [%]		Size [nm]	PDI
N1	422	30	11	40	33	0.176
N2	436	54	15	58	68	0.153
N3	442	61	12	61	79	0.15

Based on the SEM micrographs, average size of the NPs was 54 and 61 nm in N2 and N3 samples, respectively. SPR peak position is sensitive to the size of plasmonic NPs, where red shift indicates larger NPs. Comparing N2 and N3 one can see a small shift of the SPR, about 6 nm, going from N2 to N3. This indicates slightly larger particles for N3, which is estimated as 61 nm as compared to 54 nm for N2. Shortly, the scale up process has not affected the NP size significantly. DLS analyses resulted in hydrodynamic particle sizes of 68 and 79 nm, respectively. This was because the DLS analysis measures the hydrodynamic/solvodynamic diameter, which is known to be affected by the PVP coating around the Ag NPs and the interactions between this polymeric coating and ethanol. One important parameter in DLS size estimate is the polydispersity index (PDI), as it reveals the goodness of size distribution where a value less than 0.3 relates to homogeneous population. Obtained PDI values, in the order of 0.15, for samples N2 and N3 show the success of the process for both obtaining similar size NPs with a narrow size distribution. Despite the fact that the amount of the precursor in the N3 sample was twice as large as that in the N2 sample, no significant change was observed in the size and shape of the Ag NPs while larger amount of Ag NPs was synthesized in the N3 sample. Moreover, knowing that the particle size is basically determined by the balance between the nucleation and growth rate, then one may expect that any increase in the amount of $AgNO_3$for a given amount of EG increases the number of nucleation sites. In contrast to Fievet et al. [48] who suggested that, at a given temperature, the precursor-to-polyol ratio imposes no impact on the number of formed nuclei so that the number of synthesized particles remains unchanged with increasing the ratio and such an increase contributes only into the larger size of the synthesized particles, we found that the count of synthesized particles improves with increasing the amount of the precursor, rejecting the Fievet's findings. This can be attributed to the higher PVP-to-EG ratio. The PVP can, in fact, affect the performance of EG under MW irradiation because the relaxation time for a spinning EG molecule with a radius of ***r*** is expressed as follows [43]:

$$\tau = \frac{4\pi r^3 \eta}{kT} \qquad (4)$$

Therefore, $\boldsymbol{\tau}$ depends on the medium viscosity $\boldsymbol{\eta}$, and knowing that the rate constant, $\boldsymbol{k}$, is determined by the reaction molecules contact rate, then $\boldsymbol{\tau}$ is strongly associated with the intermolecular forces; PVP can affect both of these parameters. The PVP has N-methyl pyrrolidone (NMP) units, and the oxygen atoms on the polar imide group of the NMP can establish strong affinity toward the Ag^+ and facilitate the reduction of Ag^+ by electron transfer. The NMP exhibits a large dipole moment at 25℃, so that one may expect a large dielectric loss under the effect of the MW irradiation [49]. Therefore, considering the participative spinning of the molecules and the fact that the energy transfer is not attributed to a specific molecule but rather occurs as a collective phenomenon, one may consider a mean τ value that is controlled by total viscosity. Based on this explanation, the PVP offers a gradual reductive power under the MW irradiation and the EG as a strong reductive agent, and cannot reduce the number of nucleation sites and even inhibits the charge localization and hot spot formation that are known to otherwise provide preferred sites for the Ag. Moreover, upon coordination bonding between the oxygen on the carbonyl group and the Ag atoms, the N-C=O molecules are adsorbed on the surface of Ag NPs [54] and prevent the anisotropic growth. Thus, an increase in the PVP-to-EG ratio improves the number of active nucleation sites, and this can be the cause behind the formation of more spherical particles with negligible different in particle size upon the synthesis of the sample N3, as compared to the sample N2, in the tested temperature condition.

Figure 7 shows the UV-Vis and FTIR spectra recorded from the samples. The overall form of the UV-Vis plots and the presence of a single peak indicate the formation of uniformly distributed pseudo-spherical NPs. These indicate the uniform occurrence of the nucleation and crystal growth through the reaction time. With increasing the relative amount of precursor to solvent, a small shift occurred in the plasmon absorption peak from 436 nm to 442 nm, indicating the formation of slightly larger Ag NPs. Typical absorption bands for PVP were observed in the spectra for Ag NPs (Figure 7b), indicating the presence of PVP on their surface. The absorption bands of C=O and CH_2- bond stretching at 1627 cm^{-1} and1421 cm^{-1} and C-N bond vibration at 1287 cm^{-1} match the typical absorption bands of PVP. Furthermore, the absorption band of C=O bond was shifted to shorter wave numbers, indicating that the surface of Ag NPs most likely interact with the PVP via C=O groups [55]. The band around 2300 $cm^{-1}$is attributed to asymmetric stretching mode of gas phase CO_2. Thermal analysis can be used to estimate the weight ratio between the organic passivating layer and the inorganic phase. Thermal gravimetric analysis (TGA) is used for this purpose on a typical batch of Ag NPs via MW-assisted route and the resultant thermogram is presented in figure S4. The organic content decomposes and is completely lost, leaving behind only the inorganic Ag component. According to the analysis, 80% of the dried weight of is the organic layer, while 20% is AgNP content.

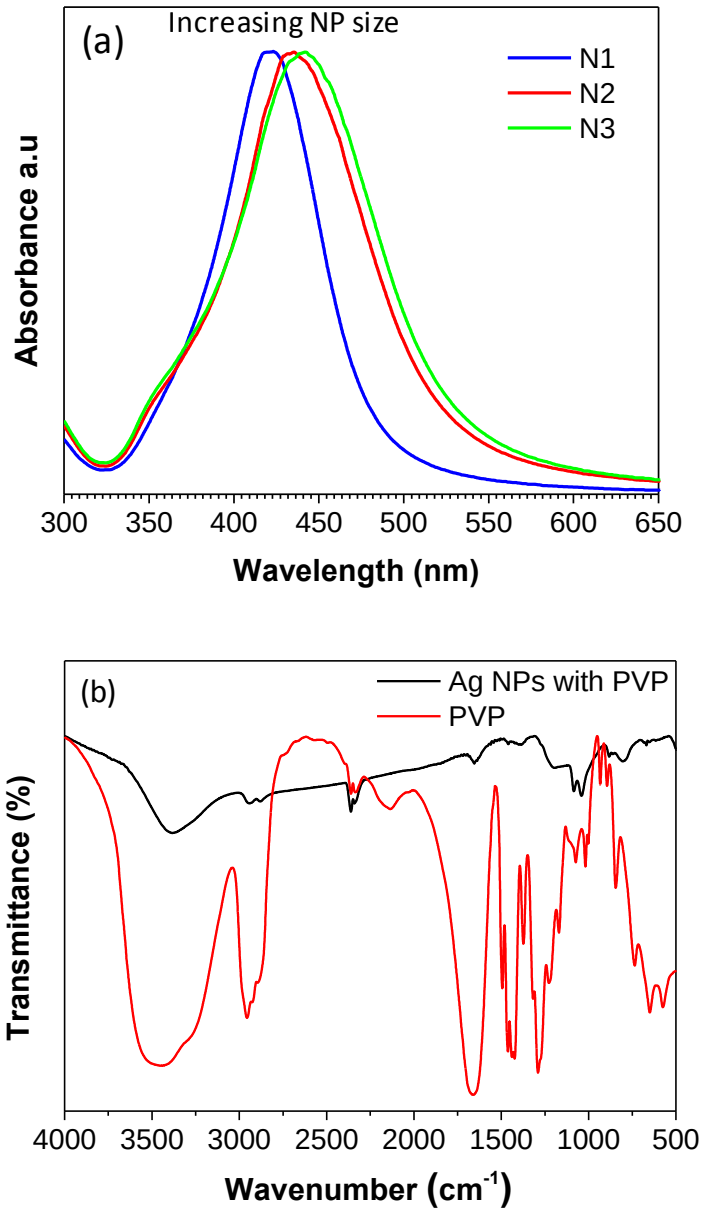

Figure 7. a) UV-Vis spectra of Ag NP samples N1-N3, and b) FTIR spectra of Ag NP along with pure the spectrum for pure PVP.

Conclusions

In this research, a new approach for the control and manipulation of both electromagnetic and thermal properties of Ag NPs, has been presented. The possibility to manage and tailor such properties at will is achieved by using our enhanced MW-assisted polyol synthesis method. A new rigorous method is developed to relate the physical (electromagnetic/thermal) characteristics of the structure with its geometrical properties. The reliability of the proposed approach has been evaluated through modeling, design, and manufacturing of AgNPs.

Ag NPs were synthesized through MW-assisted polyol method rapidly within a reaction time of only 2 min. Effects of increasing the concentration of the Ag precursor at a given amount of EG on the rate of synthesis, particle size and shape, and yield of the Ag NPs were also evaluated. At a constant PVP:$AgNO_3$ molar ratio and EG amount of 40 mL, the $AgNO_3$ concentration increased by 5 and 10 folds. The results showed that, in the MW-assisted synthesis method, the heating could be performed within a very short time, leading to homogeneous and rapid nucleation of the Ag NPs in the solution; this was acknowledged as the most important advantage of the MW-assisted heating method. With increasing the concentration of $AgNO_3$ from 0.5 to 1 g, the particle size increased from 54 nm to 61 nm, which was not significant considering the doubling of the $AgNO_3$ concentration. No change was observed in the shape of the NPs. The minor changes in the particle size indicated the activation of more nucleation sites upon the MW irradiation. Moreover, uniform and narrow distribution of the particle size, as seen on SEM images and UV-Vis spectra, was due to the fast pace and homogenous nucleation of the Ag NPs upon the MW irradiation. Using 40 mL of EG as solvent, we could synthesize about 0.3 g and 0.6 g of the Ag NPs from 0.5 g and 1 g of $AgNO_3$, respectively, indicating a significantly high yield (~90%). Increasing the amount of precursor at a given amount of solvent was found to impose no significant impact on the shape and size of the produced NPs, indicating significant differences in the chemistry of the synthesis between the MW-assisted and conventional polyol methods.

Despite the structure being experimentally verified at optical frequencies, a technique that allows the control of the particle size, shape and its physical properties is useful and of great interest in many practical applications. It is worth noting that by exploiting the proposed method we reduced the complexity in terms of synthesis process, to achieve feasible dimensions for both unit-cells and substrate thickness.

Declarations of interest: none

References

[1] M. Keshavarz Hedayati, F. Faupel, M. Elbahri, Review of plasmonic nanocomposite metamaterial absorber, Materials 7 (2014) 1221-1248; doi:10.3390/ma7021221

[2] M. A. Noginov, et al., Controlling spontaneous emission with metamaterials, Optics Letters 35 (2010) 1863-1865; doi:10.1364/OL.35.001863

[3] J. Dintinger, S. Mühlig, C. Rockstuhl, T. Scharf, A bottom-up approach to fabricate optical metamaterials by self-assembled metallic nanoparticles, Optical Materials Express 2 (2012) 269-278

[4] O. Hess, et al., Active nanoplasmonic metamaterials, Nature Materials 11 (2012) 573-584; doi: 10.1038/NMAT3356

[5] M. A. Noginov, et al., Enhancement of surface plasmons in an Ag aggregate by optical gain in a dielectric medium, Optics Letters 31 (2006) 3022-3023; doi: 10.1364/OL.31.003022

[6] M.C. Mathpal, et al., Opacity and plasmonic properties of Ag embedded glass based metamaterials, RSC Adv. 5 (2015) 12555; doi: 10.1039/c4ra14061c

[7] I. Jahan, F. Erci, I. Isildak, Microwave-assisted green synthesis of non-cytotoxic silver nanoparticles using the aqueous extract of rosa Santana (rose) petals and their antimicrobial activity, Analytical Letters 52 (2019) 1860-1873

[8] C.M. Cobley, S.E. Skrabalak, D.J. Campbell, Y. Xia, Shape-controlled synthesis of silver nanoparticles for plasmonic and sensing application, Plasmonics 4 (2009) 171-179; doi: 10.1007/s11468-009-9088-0

[9] T.A. Elwi, D.A. Jassim, H.H. Mohammed, Novel miniaturized folded UWB microstrip antenna-based metamaterial for RF energy harvesting, Int J Commun Syst. 33 (2020) 1-15; doi: 10.1002/dac.4305

[10] C. Lai, et al., Near infrared surface-enhanced raman scattering based on star-shaped gold/silver nanoparticles and hyperbolic metamaterials, SCIENTIFIC REPORTS 7 (2017) 5446; doi: 10.1038/s41598-017-05939-0

[11] J. Valentine, et al., Three-dimensional optical metamaterial with a negative refractive index, NATURE 455 (2008) 376-380; doi: 10.1038/nature07247

[12] P. Nagpal, N.C. Lindquist, S. Oh, D.J. Norris, Ultrasmooth patterned metals for plasmonics and metamaterials, Science 325 (2009) 594; doi: 10.1126/science.1174655

[13] V.A. Tamma, J. Lee, Q. Wu, W. Park, Visible frequency magnetic activity in silver nanocluster metamaterial, APPLIED OPTICS 49 (2010); doi: 10.1364/AO.49.000A11

[14] M.S. Rill, et al., Photonic metamaterials by direct laser writing and silver chemical vapour deposition, nature materials 7 (2008) 543-546; doi: 10.1038/nmat2197

[15] Z. Jie, et al., Synthesis of uniform silver nanoparticles by a microwave method in polyethylene glycol with the assistant of polyvinylpyrrolidone, Wuhan University Journal of Natural Sciences 18 (2013) 530-534; doi: 10.1007/s11859-013-0968-y

[16] S. Nandikonda, E. W.Davis, Parameters affecting microwave-assisted polyol synthesis of silver nanorods, ISRN Nanotechnology 2011 (2011); doi: 10.5402/2011/104086

[17] Z. Lalegani, S.A. Seyyed Ebrahimi, Optimization of synthesis for shape and size controlled silver nanoparticles using response surface methodology, Colloids and Surfaces A 595 (2020) 124647; doi: 10.1016/j.colsurfa.2020.124647

[18] B. Atorf, et al., Liquid crystals and precious metal: from nanoparticles dispersions to functional plasmonic nanostructures, LIQUID CRYSTALS 44 (2017) 1929-1947; doi: 10.1080/02678292.2017.1359692

[19] A. N.Naik, S. Patra, D. Sen, A. Goswami, Evaluating the mechanism of nucleation and growth of silver nanoparticles in polymer membrane under continuous precursor supply: tuning of multiple to single nucleation pathway, Phys. Chem. Chem. Phys. 21 (2019) 4193-4199; doi: 10.1039/C8CP06202A

[20] M. Torras, A. Roig, From silver plates to spherical nanoparticles: snapshots of microwave-assisted polyol synthesis, ACS Omega 5 (2020) 5731-5738; doi: 10.1021/acsomega.9b03748

[21] N. Dahal, S. Garcia, J. Zhou, S. M.Humphery, Beneficial effects of microwave-assisted heating versus conventional heating in noble metal nanoparticles synthesis, ACS Nano 6 (2012) 9433-9446; doi: 10.1021/nn3038918

[22] B. Hamawandi, et al., Composition tuning of nanostructured binary copper selenides through rapid chemical synthesis and their thermoelectric property evaluation, Nanomaterials 10 (2020) 754; doi: 10.3390/nano10050854

[23] C. Xue, et al., Current status of applying microwave-assisted catalysis for the degradation of organics in aqueous phase – A review, JOURNAL OF ENVIROMENTAL SCIENCES 81 (2019) 119-135; doi: 10.1016/j.jes.2019.01.019

[24] Y. Asakuma, S. Matsumura, A. Saptoro, Method for suppressing superheating behavior during microwave assisted nanoparticles formation by ethylene glycol addition, Chemical Engineering & Processing: Process Intensification 132 (2018) 11-15; doi: 10.1016/j.cep.2018.08.003

[25] B. Hamawandi, et al., Facile solution synthesis, processing and characterization of n- and p- type binary and ternary Bi-Sb tellurides, Appl. Sci. 10 (2020) 1178; doi: 10.3390/app10031178

[26] D. Su, et al., Microwave assisted green synthesis of pectin based silver nanoparticles and their antibacterial and antifungal activities, Materials Letters 244 (2019) 35-38; doi: 10.1016/j.matlet.2019.02.059

[27] H. Ashraf, T. Anjum, S. Riaz, S. Naseem, Microwave-assisted green synthesis and characterization of silver nanoparticles using melia azedarach for the management of fusarium wilt in tomato, Frontiers in Microbiology 11 (2020); doi:10.3389/fmicb.2020.00238

[28] Z. Yi, et al., Microwave-assisted polyol method rapid synthesis of high quality and yield Ag nanowires, Surface & Coating Technology 327 (2017) 118-125; doi: 10.1016/j.surfcoat.2017.08.024

[29] T. Darmanin, et al., Microwave-assisted synthesis of silver nanoprisms/nanoplates using a “modified polyol process”, Colloids and Surfaces A: Physicochem. Eng. Aspects 395 (2012) 145-151; doi: 10.1016/j.colsurfa.2011.12.020

[30] G. Dzido, et al., Rapid continuous microwave-assisted synthesis of silver nanoparticles to achieve very high productivity and full yield: from mechanistic study to optimal fabrication strategy, J Nanopart Res 17 (2015); doi: 10.1007/s11051-014-2843-y

[31] J. Helmlinger, et al., A rapid, high-yield and large-scale synthesis of uniform spherical silver nanoparticles by a microwave-assisted polyol process, RSC Adv 5 (2015) 92144-92150; doi: 10.1039/C5RA20446A

[32] P. Saloga, C. Kästner, A. Thünemann, High-speed but not magic: microwave-assisted synthesis of ultra-small silver nanoparticles, Langmuir 34 (2018) 147-153; doi: 10.1021/acs.langmuir.7b01541

[33] S. Kumar, et al., High conversion synthesis of < 10nm starch-stabilized silver nanoparticles using microwave technology, SCIENTIFIC REPORTS 8 (2018) 5106; doi: 10.1038/s41598-018-23480-6

[34]P. Moon, D. E. Spencer, Field Theory Handbook, Berlin, Germany, Springer-Verlag, 1963

[35] S. Jhung, T. Jin, Y. Hwang, J. Chang, Microwave effect in the fast synthesis of microporous materials: which stage between nucleation and crystal growth is accelerated by microwave irradiation?, Chem. Eur. J. 13 (2007) 4410-4417; doi: 10.1002/chem.200700098

[36] A. Harrison, A.G. Whittaker, Microwave heating, Comprehensive Coordination Chemistry II 1 (2003) 741-745; doi: 10.1016/B0-08-043748-6/01162-2

[37] V. Chikan, E. McLaurin, Rapid nanoparticles synthesis by magnetic and microwave heating, Nanomaterials 6 (2016); doi: 10.3390/nano6050085

[38] A. Grewal, K. Kumar, S. Redhu, S. Bhardwaj, Microwave assisted synthesis: A green chemistry approach, Int. Res J Pharm. App Sci. 3 (2013) 278-285

[39] D. El Khaled, N. Novas, J.A. Gazquez, F. Manzano-Agugliaro, Microwave dielectric heating: Applications on metals processing, Renewable and Sustainable Energy Review 82 (2018) 2880-2892; doi: 10.1016/j.rser.2017.10.043

[40] S.M. Kazemzadeh, A. Hassanjani-Roshan, M.R. Vaezi, A. Shokuhfar, The effect of microwave irradiation time on appearance properties of silver nanoparticles, Transactions of The Indian Institute of Metals 64 (2011) 261-264; doi: 10.1007/s12666-011-0053-1

[41] M. Gawande, S. Shelke, R. Zboril, R. Varma, Microwave-assisted chemistry: Synthesis applications for rapid assembly of nanomaterials and organics, Acc. Chem. Res. 47 (2014) 1338-1348; doi: 10.1021/ar400309b

[42] M. Doreth, et al., Influence of PVP molecular weight on the microwave assisted in situ amorphization of indomethacin, European Journal of Pharmaceutics and Biopharmaceutics 122 (2018) 62-69; doi: 10.1016/j.ejpb.2017.10.001

[43] C. Gabriel, et al., Dielectric parameters relevant to microwave dielectric heating, Chemical Society Reviews 27 (1998) 213-224; doi: 10.1039/A827213Z

[44] T. Tripathy, B.R. De, Making sense about dipole moments, Journal of Physical Sciences 12 (2008) 155-172

[45] R.J. Sengwa, K. Kaur, R. Chaudhary, Dielectric properties of low molecular weight poly (ethylene glycol)s, PolymInt 49 (2000) 599-608

[46] P.B. Undre, et al., Dielectric relaxation in ethylene glycol – dimethyl sulfoxide mixtures as a function of composition and temperature, Journal of the Korean Chemical Society 56 (2012) 416-423; doi: http://dx.doi.org/10.5012/jkcs.2012.56.4.416

[47] R.J. Sengwa, S. Sankhla, Characterization of ionic conduction and electrode polarization relaxation processes in ethylene glycol oligomers, Polymer Bulletin 60 (2008) 689-700; doi: 10.1007/s00289-008-0892-z

[48] F. Fievet, J.P. Lagier, B. Blin, Homogeneous and heterogeneous nucleations in the polyol process for the preparation of micron and submicron size metal particles, Solid State Ionics 32/33 (1989) 198-205; doi: 10.1016/0167-2738(89)90222-1

[49] S.Mukherji, S. Bharti, G. Shukla, S. Mukherji, Synthesis and characterization of size and shape controlled silver nanoparticles, Physical Sciences Reviews (2018) 20170082; doi: 10.1515/psr-2017-0082

[50] P. A.Mello, J. S.Barin, R. A.Guarnieri, Microwave-assisted sample preparation for trace element analysis, (2014) 59-75; doi: 10.1016/B978-0-444-59420-4.00002-7

[51] M. Nüchter, B. Ondruschka, W. Bonrath, A. Gum, Microwave assisted synthesis – a critical technology overview, Green Chem. 6 (2004) 128-141; doi: 10.1039/b310502d

[52] C. Luo, et al., The role of poly (ethylene glycol) in the formation of silver nanoparticles, Journal of Colloid and Interface Science 288 (2005) 444-448; doi: 10.1016/j.jcis.2005.03.005

[53] Oldenburg, S. J. Light Scattering from Gold Nanoshells. Diss. Rice University, 2000 https://nanocomposix.com/pages/mie-theory-calculator#target

[54] D. M, M. Revathi, L. M, Microwave synthesis of silver nanoparticles by polyol method and testing their synergistic antibacterial activity in the presence of vancomycin, Asian Journal of Pharmaceutical and clinical research 11 (2018) 288-298; doi: 10.22159/ajpcr.2018.v11i10.27174

[55] Koczkur, Kallum M., et al. "Polyvinylpyrrolidone (PVP) in nanoparticle synthesis." *Dalton Transactions* 44.41 (2015): 17883-17905.